Supporting Information

Tailoring capping-layer composition for improved stability of mixed-halide perovskites

Noor Titan Putri Hartono[1], Marie-Hélène Tremblay[2], Sarah Wieghold[3], Benjia Dou,[1] Janak Thapa[1], Armi Tiihonen[1], Vladimir Bulovic[1], Lea Nienhaus[4], Seth R. Marder[2,5-8]*, Tonio Buonassisi[1]*, Shijing Sun[1]**

Affiliations:

[1]Massachusetts Institute of Technology, 77 Massachusetts Avenue, Cambridge, MA 02139

[2]Georgia Institute of Technology, North Avenue, Atlanta, GA 30332

[3]Argonne National Laboratory, 9700 S. Cass Avenue, Lemont, IL 60439

[4] Florida State University, Department of Chemistry and Biochemistry, 95 Chieftan Way Tallahassee, FL 32306

[5]University of Colorado Boulder, Renewable and Sustainable Energy Institute, Boulder, CO 80303

[6]University of Colorado Boulder, Department of Chemical and Biological Engineering, Boulder, CO 80303

[7]University of Colorado Boulder, Department of Chemistry, Boulder, CO 80303

[8]National Renewable Energy Laboratory, Chemistry and Nanoscience Center, Golden, CO 80401

*Correspondence to: NTPH (nhartono@mit.edu, noortitan@alum.mit.edu), SRM (Seth.Marder@colorado.edu), TB (buonassisi@mit.edu), SS (shijings@mit.edu)

Discussion on the underlying scientific mechanisms of the degradation

Looking at the stressors present during degradation: illumination, humidity, oxygen, and heat, we identify 4 possible mechanisms of degradation: anion drift, the breakdown of organics (including deprotonation of *A*-site cations), crystal structure/perovskite layer change, and oxygen adsorption.

The following 3 possible degradation mechanisms cannot be concluded based on the current data, and are presented for discussion purpose.

The breaking down of organic *A*-site cations is the next possible degradation mechanism, especially the ones coming from 2D/1D perovskite undergoing deprotonation. The *A*-site cations lose H^+ and convert the ammonium cation into amine, which is already investigated in the case of phenethylammonium cation.[1,2] Note that the deprotonation cannot happen in quaternary ammonium such as phenyltriethylammonium ($PTEA^+$) in PTEAI. The rest of the capping layers explored has primary ammonium, and thus, can undergo deprotonation. The pK_a measures how likely a compound gives up a proton; therefore, low pK_a corresponds to a stronger acid, with higher likelihood for the compound to give up a proton. Based on the simulated pK_a values for 1D organics *A*-site cations, 4-I ($2NO_2$-PEA-I) is more likely to give up its proton (pK_a = 9.35), while 9-Cl (2MeI-NEA-Cl) and 6-I (3MeO-PEA-I) are less likely to be deprotonated (pK_a = 9.92 and 9.99, respectively). On the other hand, the branches breaking down from relatively stable phenyl/naphthyl rings in the capping *A*-site cations is unlikely to happen, because their reactions are kinetically not favorable. These reactions require higher energy, and sometimes, a very basic or acidic condition to proceed.

The crystal structures and perovskite layers also possibly change during degradation process, similar to the case of Ruddlesden-Popper perovskite that has its *n* number of layers reduced due to the presence of water.[1,3] Depending on how thermodynamically stable these secondary phases are, these could accelerate or decelerate the degradation process.[3] For instance, in the case of butylammonium iodide, the secondary phases are stoichiometrically more hydrophobic, which improves the material stability.[3]

Another degradation pathway is driven by oxygen adsorption, that eventually turns into superoxide formation.[4] It is initiated by generation of superoxide anions under light, that oxidizes the perovskite surface and slowly hydrates the inner perovskite, despite the very low humidity condition. Investigating the likelihood of low-dimensional perovskites getting oxidized in future studies will be required in unravelling how capping layer materials might help to suppress the oxygen adsorption-based degradation.

It is challenging to pinpoint which degradation mechanism dominates among these 4 when all the stressors are present during the aging test. it is highly likely that the dominating degradation mechanism differs across 1D capping layer materials, and across the mixed-halide absorbers.

Samples	**Value at time = 0 mins.**	**Value at time = 3 mins.**	**Value at time = 6 mins.**
X (1)	120	150	180
X (2)	140	170	180
Y (1)	100	90	120
Y (2)	125	125	140
Z	130	125	130

Supporting Table S1. The hypothetical dataset, and the dissimilarity matrix analysis is shown in Supporting Figure S1.

Devices	Voc [mV]	Jsc [mA/cm^2]	FF [%]	PCE [%]
Bare $MAPbI_3$	1089	21.6	72.67	17.1
Bare $MAPb(I_{0.75}Br_{0.25})_3$	677.7	13.29	38.3	3.449
9-Cl-capped $MAPbI_3$	1079	18.38	44.19	8.761
9-Cl-capped $MAPb(I_{0.75}Br_{0.25})_3$	976	12.18	44.91	5.34

Supporting Table S2. The best device performance for bare and 9-Cl capped $MAPbI_3$, as well as bare and 9-Cl-capped $MAPb(I_{0.75}Br_{0.25})_3$.

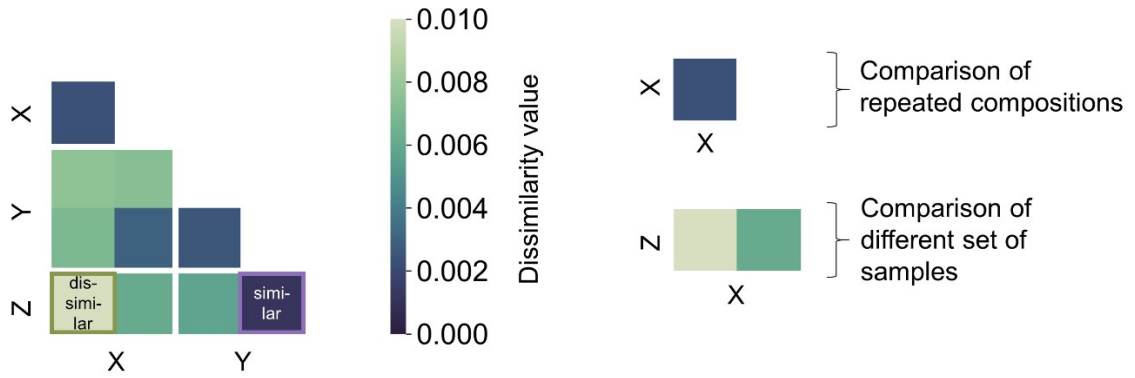

Supporting Figure S1. The hypothetical example of dissimilarity matrix result using cosine metric, based on data from Supporting Table S1.

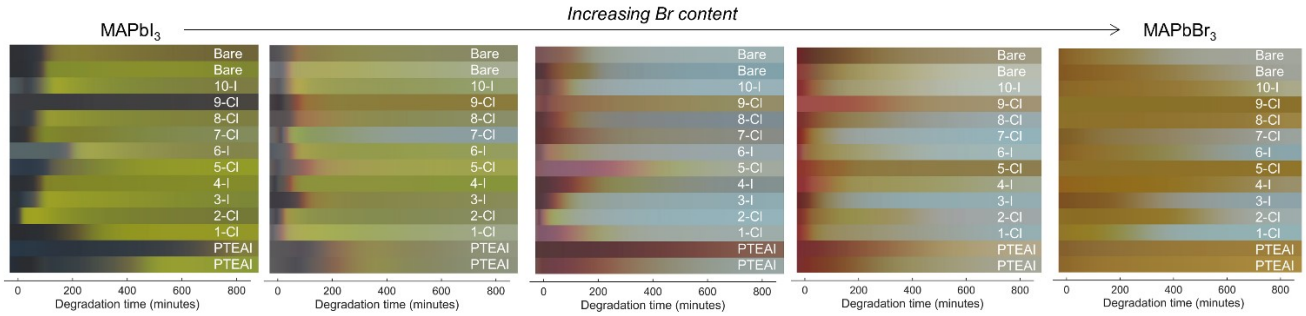

Supporting Figure S2. The degradation result for various capping layer materials in different absorbers.

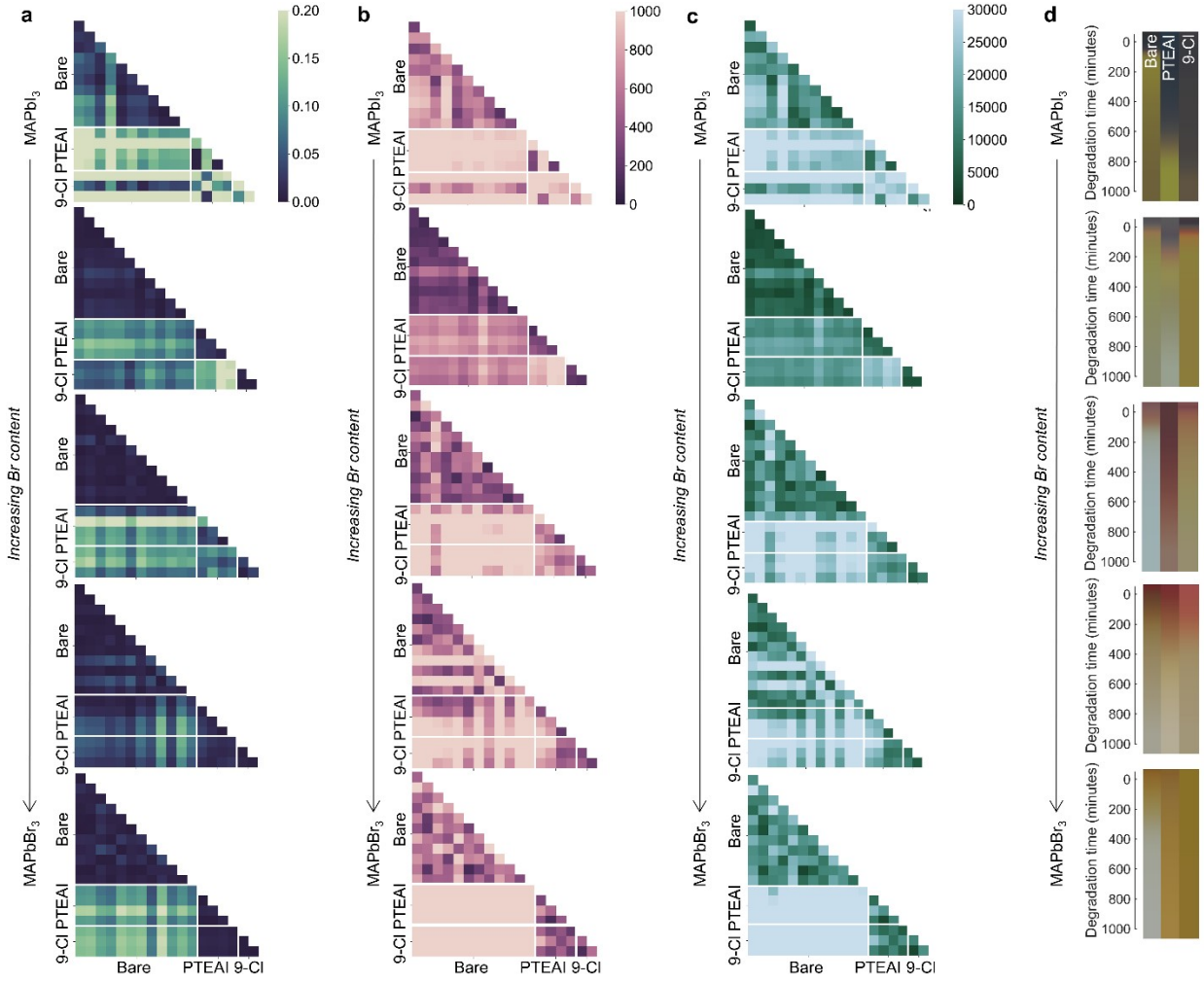

Supporting Figure S3. The dissimilarity matrices using **a.** cosine, **b.** Euclidean, and **c.** Manhattan distance measures.

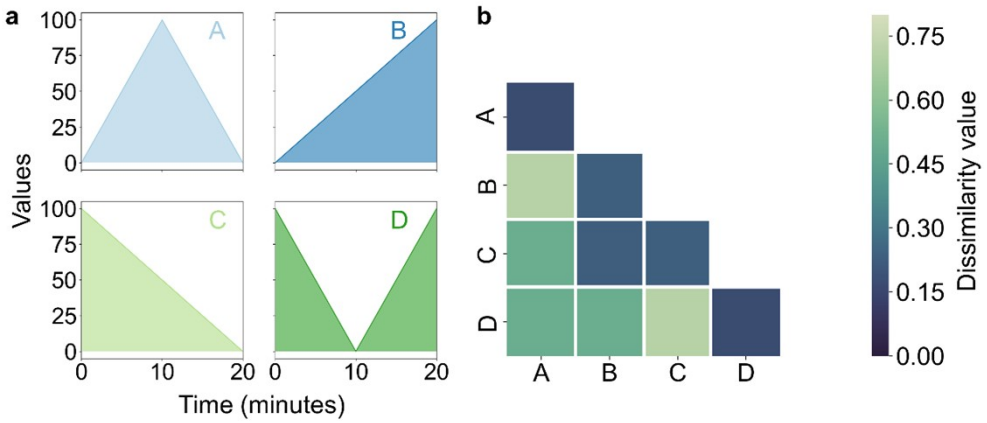

Supporting Figure S4. **a.** The example of hypothetical RGB values change over time, with the same area under the curve, which results in the same instability index, but actually has different colors. **b.** The dissimilarity matrix highlighting the differences across samples.

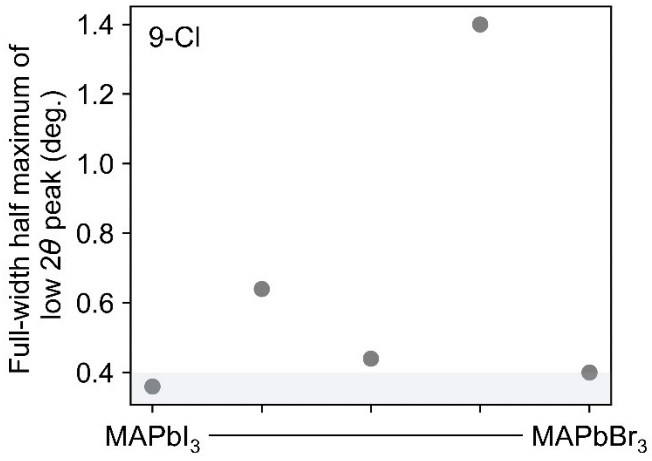

Supporting Figure S5. The full-width half maximum of low 2θ-angle peak in 9-Cl-capped films.

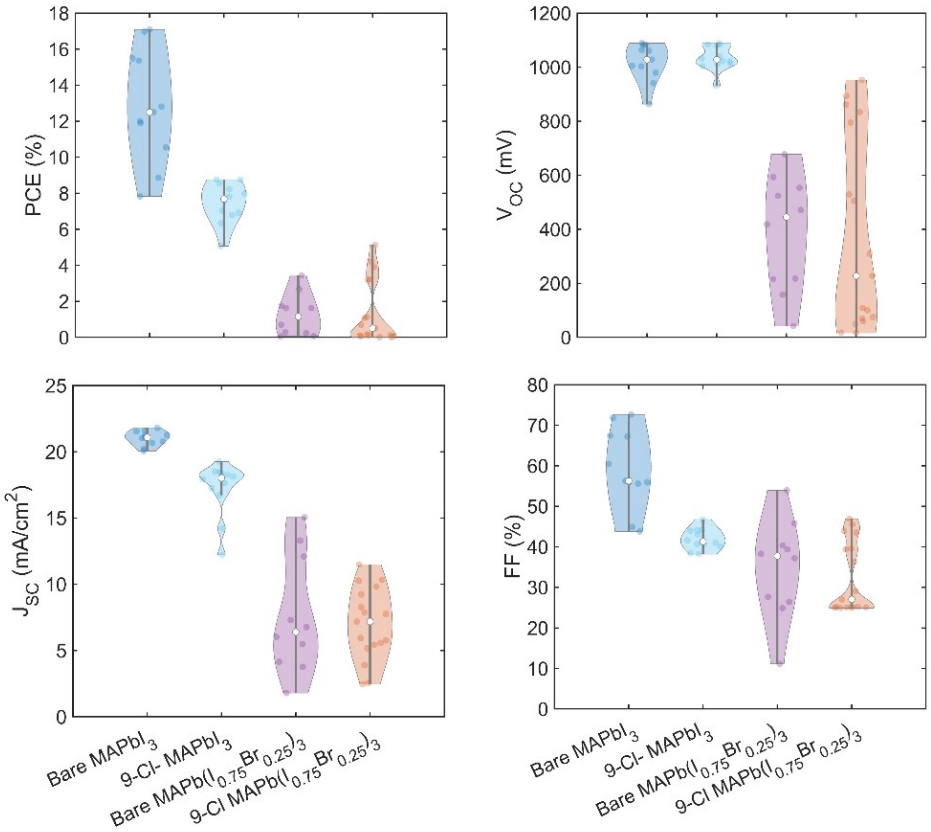

Supporting Figure S6. The device performance (reverse) for 9-Cl-capped and bare MAPb(I_xBr_{1-x})$_3$ for x = 1 and 0.75.

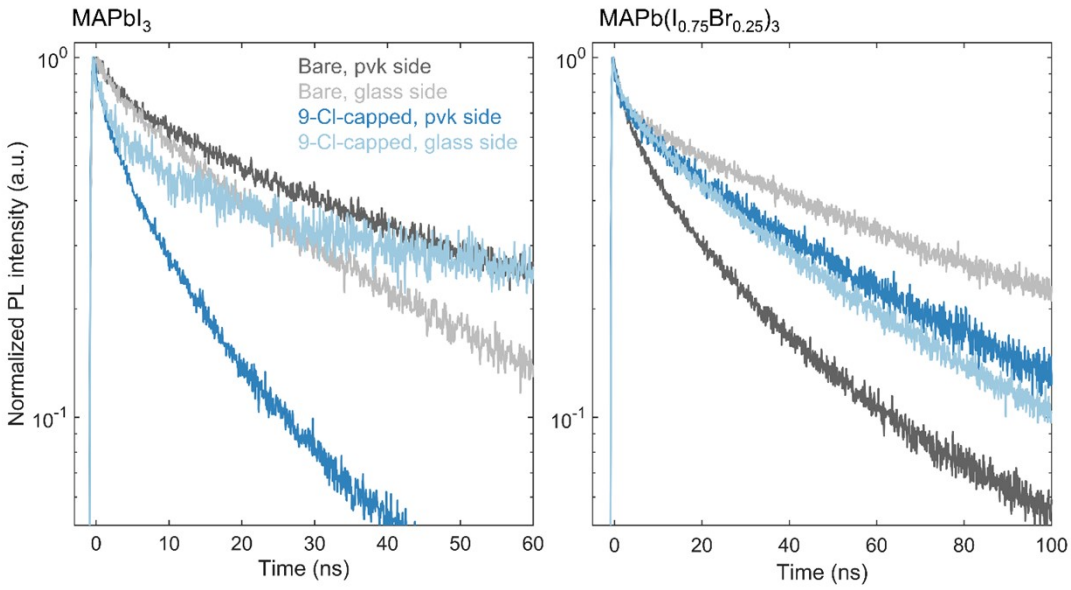

Supporting Figure S7. The time-resolved photoluminescence (TRPL) of the 9-Cl-capped and bare $MAPb(I_xBr_{1-x})_3$ for x = 1 and 0.75.

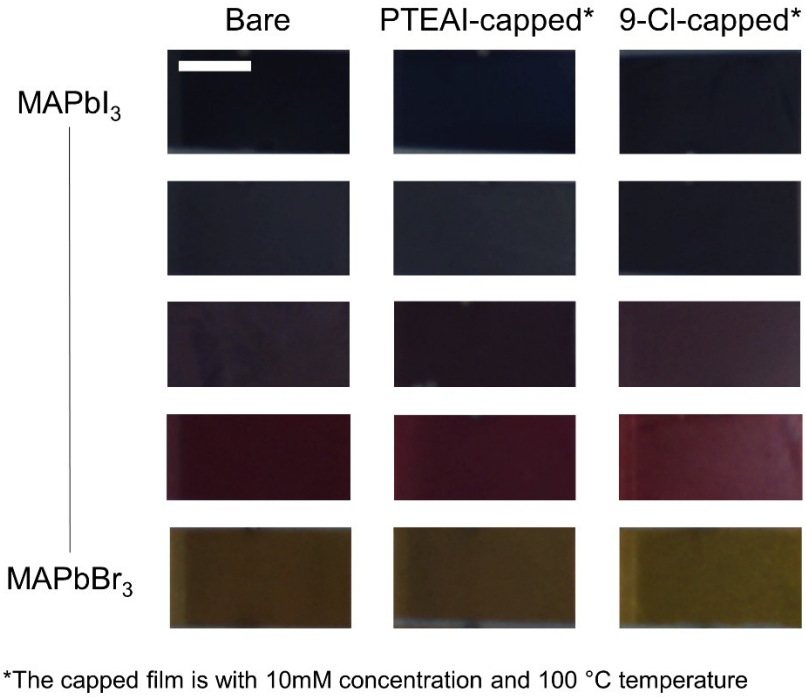

Supporting Figure S8. The initial color of the films for bare, PTEAI-capped, and 9-Cl-capped films of $MAPb(I_xBr_{1-x})_3$ for x = 1, 0.75, 0.5, 0.25, and 0. The scale bar is 1 cm.

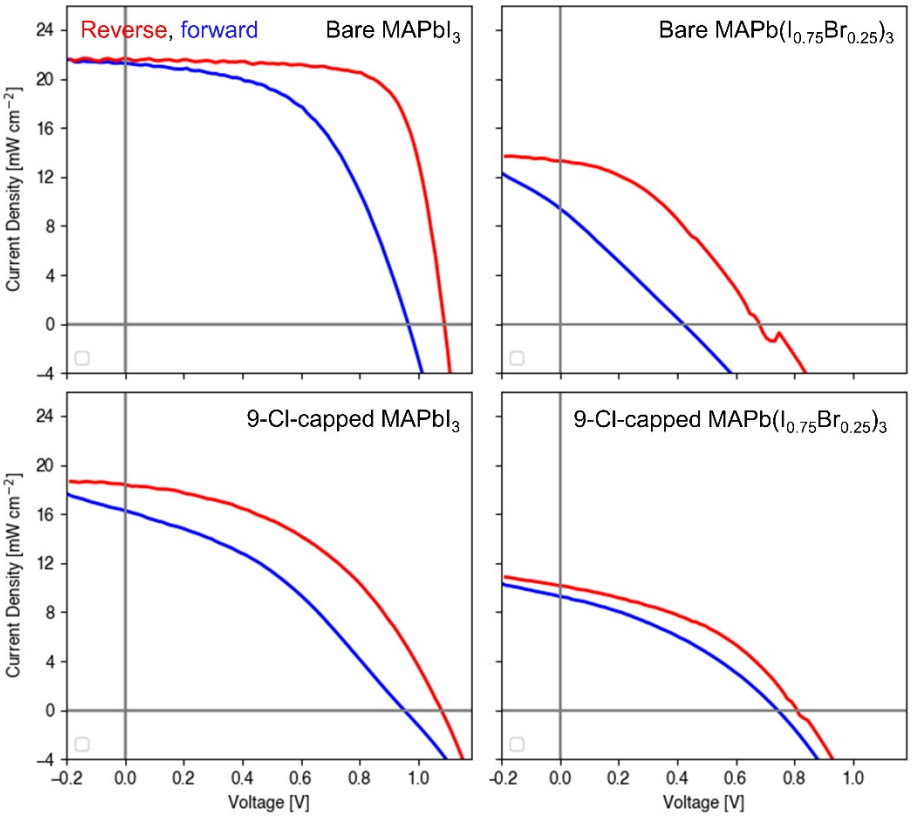

Supporting Figure S9. The *JV* curve for bare and 9-Cl capped $MAPbI_3$, as well as bare and 9-Cl-capped $MAPb(I_{0.75}Br_{0.25})_3$.

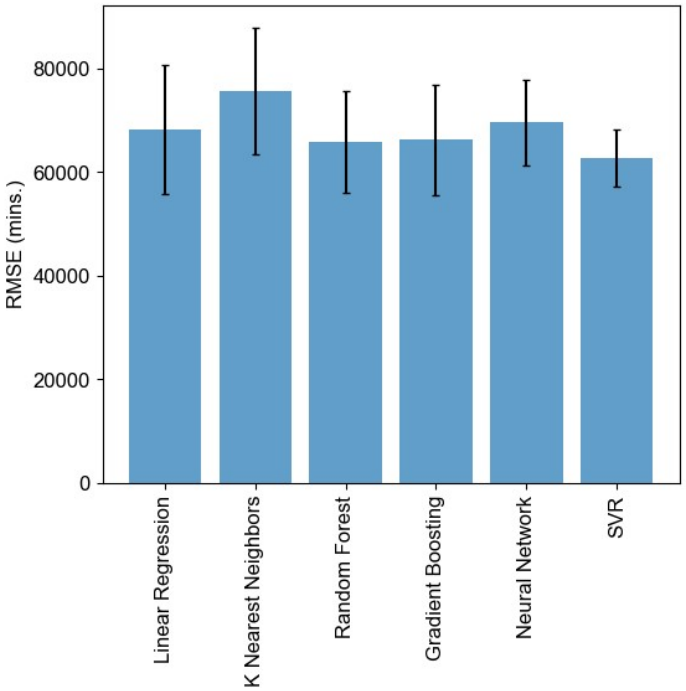

Supporting Figure S10. The root mean squared error (RMSE) results across different algorithms.

References

1 J. Schlipf, Y. Hu, S. Pratap, L. Bießmann, N. Hohn, L. Porcar, T. Bein, P. Docampo and P. Müller-Buschbaum, *ACS Appl. Energy Mater.*, 2019, **2**, 1011–1018.

2 H.-H. Fang, J. Yang, S. Tao, S. Adjokatse, M. E. Kamminga, J. Ye, G. R. Blake, J. Even and M. A. Loi, *Adv. Funct. Mater.*, 2018, **28**, 1800305.

3 B. R. Wygant, A. Z. Ye, A. Dolocan, Q. Vu, D. M. Abbot and C. B. Mullins, *J. Am. Chem. Soc.*, 2019, **141**, 18170–18181.

4 Y. Ouyang, Y. Li, P. Zhu, Q. Li, Y. Gao, J. Tong, L. Shi, Q. Zhou, C. Ling, Q. Chen, Z. Deng, H. Tan, W. Deng and J. Wang, *J. Mater. Chem. A*, 2019, **7**, 2275–2282.